Regular Article

PHYSICAL CHEMISTRY RESEARCH
Published by the
Iranian Chemical Society
www.physchemres.org
info@physchemres.org

Phys. Chem. Res., Vol. 9, No. 4, 553-564, December 2021
DOI: 10.22036/pcr.2021.270358.1878

Photocatalytic and Optical Performances of CeO_2 by Substitution of Titanium

H.A. Miran*, Z.N. Jaf, I.H. Khaleel and A.A. Alkhafaji
Department of Physics, College of Education for Pure Science/Ibn-Al-Haitham, University of Baghdad, Baghdad, Iraq
(Received 26 January 2021, Accepted 14 May 2021)

In this contribution, density functional theory-based calculations were carried out to assess the electronic, photocatalytic and optical properties of $Ce_{1-x}Ti_xO_2$ system. Ti incorporation resulted in a decrease in Ce 4*f* states and an increase in Ti 3*d* states in the bottom of conduction band. Furthermore, it was found that doping ceria with Ti-like transition metals could evidently shift the absorption of pure CeO_2 towards the higher wavelength range. These findings can provide some new insights for designing CeO_2-based photocatalysts with high photocatalytic performance. To the best of our knowledge, this investigation calculates the Mullikan charge transfer of $Ce_{1-x}Ti_xO_2$ system for the first time. Charge transfer reveals an ionic bond between Ce or Ti and O, and covalent bonds between Ce and Ti atoms in the studied systems.

Keywords: Rare earth oxides (REOs), Cerium oxide (CeO_2), Computational modeling, Density functional theory (DFT), Density of states (DOSs), Ti-doping

INTRODUCTION

Over the past decades, a great deal of research has been concentrated on rare-earth oxides (REOs) [1,2]. Their partially filled 4*f* and 5*d* orbitals cause high electrical conductivity and thermal stability [3]. Cerium (Ce) has unusual characteristics linked to the presence of only one 4*f* electron in addition to the 5*d* filled state. Cerium oxide (CeO_2) containing materials have been gaining great scientific interest due to demonstrating a number of extraordinary properties which directly depend on the presence of point defects; *i.e.*, oxygen vacancies generated due to reducing Ce^{4+} to Ce^{3+} oxidation state [4]. For instance, epitaxial CeO_2 films were fabricated as the buffer layers for high temperature superconducting [5]. Furthermore, cerium oxide thin films utilized as high-*k* dielectric material in capacitors. In addition, CeO_2-based electrodes were developed for solid oxide fuel cells [6] and rare earth was also found to improve optical and photoconductivity properties of CdS [7]. In addition, CeO_2 nanoparticles were utilized as antioxidant agents [8]. Owing to the distinctive redox properties and high oxygen storage capacity, CeO_2 is widely used as catalysts [9,10]. It is reported that CeO_2 with the cubic fluorite structure possesses a wide band gap energy of 3.2 eV which limits its photocatalytic activity under the ultraviolet (UV) radiation [11]. It is suggested that the transition metal doped CeO_2 nanoparticles enhance the UV absorption properties [12]. Yue *et al.* [13] stated that introducing some impurities (dopants) ions such as Ti, Mn , Fe and Co within the CeO_2 lattice enhances its photocatalytic properties and promotes the narrowing of the band gap to the visible photocatalytic characteristics leading to a significant absorption shifts towards the visible region. Truffault *et al.* [14] synthesized Calcium(Ca)-doped CeO_2 nanoparticles with doping concentrations between 0 and 50 mol% for the short ultraviolet type A radiation filtration application. Channei *et al.* [15] proposed that Fe-doped CeO_2 films exhibit superior photocatalytic performances compared to the pure CeO_2 films due to decreasing in band gap energy and increasing the specific surface area. Furthermore,

*Corresponding author. E-mail: hussein.a.j@ihcoedu.uobaghdad.edu.iq

hydrothermal synthesis approach has been used to prepare Yttrium (Y)-doped CeO_2 nanorods for the degradation of indigo carmine dyes [16]. Results indicated that the photocatalytic activity increased by increasing the doping content of Y until reaching a specific doping level and additional increasing in the doping contents may result in decreasing the photocatalytic activity. The greatest improvement in photocatalytic activity is ascribed to the creation of oxygen vacancy into CeO_2 up to a certain limit of Y loading. However, increasing the optimum doping level showed reducing in photocatalytic activity. In another study, the effect of Samarium (Sm) doping on the structural, surface morphological, and optical properties of CeO_2 nanoparticles has been investigated [17]. They indicated that controlled band gap, size, grain morphology, extrinsic and intrinsic oxygen vacancies in the Sm-doping CeO_2 lattice promote these nanoparticles to be appropriate replacements for various applications. Further, it has been reported that doping with transition metal such as Fe, Co, and Ni was implemented to create oxygen vacancies in CeO_2 and enhanced activity for carbonyl sulfide hydrolysis. The strong interaction between doped metals and CeO_2 encourages the spontaneous generation of asymmetric oxygen vacancies in metal doped CeO_2 nanorods. These asymmetric oxygen vacancies would assist the activation and dissociation of H_2O and generation of active hydroxyls, contributing to improve the activity for COS hydrolysis [18]. Moreover, the effect of various loadings of Cu ions into the CeO_2 lattice is proven to enhance the optical and visible photocatalytic properties of CeO_2. In addition, the visible photocatalytic degradation of methylene blue in the presence of 7 wt% Cu-doped CeO_2 nanoparticles revealed the degradation rates about 1.41×10^{-2} min^{-1} and 1.12×10^{-2} min^{-1} under the exposure to natural sunlight and visible light, correspondingly [19].

From theoretical view point, a research group examined the enhancement in visible light photocatalytic performance of transition metals (Fe, Cr and Co)-doped CeO_2 nanomaterials. It was demonstrated that the reduced band gap and strong absorption induced by impurity levels are responsible for the enhanced visible-light photocatalytic activity of doped CeO_2 [20]. Moreover, density functional theory (DFT) demonstrated a powerful tool to explore the adsorption of SO_2 molecules over Ir/P-modified graphitic carbon nitride (gCN) to present pertinent systems that operate in sensing and eliminating SO_2 molecules from atmosphere. The findings of PDOS plots revealed that the sharp peak is localized near the Fermi energy level in SO_2-adsorbed Ir/P-modified gCN system, which confirmed the strong adsorption of SO_2 molecules on the studied system [21]. Another DFT study predicted that the band gap energy of graphitic carbon nitride (g-C_3N_4) decreased significantly by metal insertion of Ni, Pd and Pt [22].

First-principle calculations also implemented to inspect the effect of Hf and Zr loadings on the reduction enthalpies of CeO_x configurations. In an agreement with XRD measurements, alloying these metals to the stoichiometric and reduced CeO_2 lattice correlates with the reduction in their volume cells. Furthermore, reduces their reduction enthalpy, and hence displaying an enhancement in the catalytic activities of Hf/Zr-CeO_2 systems [23].

To this end, this computational work aims to investigate the effect of transition metal of Ti on the photocatalytic and optical characteristics of CeO_2. Furthermore, Mulliken population analysis is considered to compute the charge transfer for the individual atoms in molecules of the systems, and thereafter, exploring the bonding character between the constituents in the molecules. In this study, Ti as a dopant was selected owing to its smaller ionic radius than Ce and easily replacing in Ce lattice.

METHOD OF CALCULATIONS

The calculations were achieved with the Cambridge serial total energy package (CASTEP) code, based on the density functional theory [24]. Owing to the strong Coulomb interaction of the localized Ce 4*f* electrons, the standard density functional theory (DFT) calculations underestimate the band gap [25]. Hence, density functional correlated (GGA + U) calculations were applied in this study. Moreover, based on the default setting of CASTEP software, the value of the utilized Hubbard parameter (U) corresponds to 6.0 eV and 2.5 eV for Ce and Ti, respectively. Electron-ion interactions were described through ultrasoft pseudopotentials in reciprocal space with valence electron configurations of $2s^2$ $2p^4$ for oxygen, $3d^2$ $4s^2$ for titanium atom and $4f^1$ $5s^2$ $5p^6$ $5d^1$ $6s^2$ for cerium. Initially, the calculations were performed at a supercell of

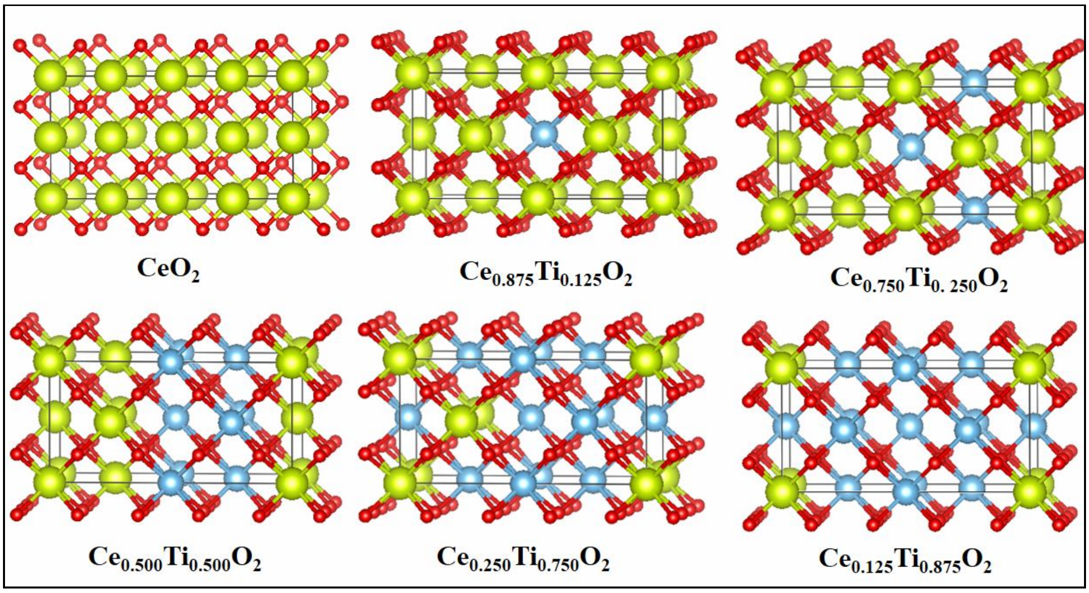

Fig. 1. The relaxed supercell structures of $Ce_{1-x}Ti_xO_2$ systems plotted by means of VESTA visualization software. The light green spheres refer to Ce, red spheres correspond to O, and the light blue denotes to Ti atoms.

2×1×1 comprised of 8-cerium atoms and 16 oxygen atoms. To set the Ti-doped models, the substitutional method was implemented at x = 0.125, 0.250, 0.500, 0.750 and 0.875. Suggesting that at x = 0.125, only one Ce atom has been substituted by Ti, at x = 0.250, two Ce atoms are substituted, at x = 0.500 four Ce atoms are replaced, at x = 0.750 six Ce atoms are replaced, and at x = 0.875 seven Ce atoms are replaced by Ti.

In a similar manner, the $Ce_{1-x}T_xO_2$ system corresponds to Ce concentration of x = 0.125, 0.25, 0.500, 0.750, 0.875 as disclosed in Fig. 1. The total energy was minimized for CeO_2 using a set of k-points in the irreducible sector of Brillouin zone, equivalent to a 3×2×2 Monkhorst-Pack grid in the unit cells, and a cutoff energy of 300 eV. The convergence tolerance of energy was set at 5.0×10^{-6} eV/atom. Regarding the optimization process, the energy change, maximum force, maximum stress, and maximum displacement tolerances were set as 1×10^{-6} eV/atom, 0.03 eV/Å, 0.05 GPa, and 0.001 Å, correspondingly. Finally, the scissor operator of 0.98 eV was applied to reproduce the measured electronic band gap [26,27]. This value of scissors operator was implemented to all the subsequent optical calculation.

RESULTS AND DISCUSSION

Geometry Optimization of Pure and Ti-doped CeO_2

The optimized supercells of pure and Ti- doped CeO_2 are shown in Fig. 1. It is well known that CeO_2 displays a cubic fluorite lattice with the space group of Fm-3m which is composed of four formula units in a unit cell (*i.e.*, 4 cerium and 8 oxygen atoms). Our simulated findings of the lattice parameters are in accordance with that of the experimentally measured value of a = 5.410 Å. These results correspond well with those in the previously published work [28].

The lattice parameters and Mulliken population results of the optimized configurations are reported in Table 1. The lattice parameters values of the optimized configurations decreased with the increasing Ti-doping concentration. This is ascribed to a noticeable lattice distortion while introducing Ti ions.

Table 1 lists Mulliken charges on Ce, O and Ti atoms in $Ce_{1-x}Ti_xO_2$ system. From the table, it is observed that Ce and Ti atoms in the simulated structures hold positive charges while O atoms are associated with negative charges. Our

Table 1. The Calculated Lattice Constants (Å), Formation Energy for the Studied Systems (eV), Band Gap (eV) and Charge Transfer (e) for Pure and Ti-doped CeO_2 Configurations

Configuration	Lattice constants (Å)	Formation energy (eV)	Band gap (eV)	Charge transfer (e)		
				Ce	Ti	O
CeO_2	a = 5.41	-1.94×10^3	3.19	1.27	-	-0.63
$Ce_{1-x}Ti_xO_2$, x = 0.125	a = 5.39	-1.60×10^4	2.88	1.33	1.03	-0.65
$Ce_{1-x}Ti_xO_2$ x = 0.250	a = 5.35	-1.66×10^4	2.67	1.36	1.08	-0.65
$Ce_{1-x}Ti_xO_2$ x = 0.500	a = 5.18	-1.76×10^4	2.33	1.37	1.15	-0.65
$Ce_{1-x}Ti_xO_2$ x = 0.750	a = 5.04	-1.87×10^4	2.28	1.56	1.20	-0.66
$Ce_{1-x}Ti_xO_2$ x = 0.875	a = 4.91	-1.93×10^4	2.19	1.57	1.24	-0.62

analysis of Mulliken charge values indicates a covalent character for Ti-Ce bond in all the simulated systems that have Ti and Ce atoms and ionic characteristics for Ti-O and Ce-O bonds. Moreover, these results demonstrate that Ce atoms loss more electrons when introducing Ti into the system, whereas the electron gains of O atoms are almost steady when Ti contents increased [29].

Density of States (DOSs) Analysis

To investigate the electronic properties of $Ce_{1-x}Ti_xO_2$ system, the electronic density of states (DOSs) of the optimized supercells is demonstrated in Fig. 2. Our findings show that the CeO_2 structure displays a nonmetallic nature, which indicates a semiconducting character. The Fermi level is located at zero energy to easily recognize the band gap. For x = 0 (pure CeO_2 configuration), DOS of CeO_2 agreed well with the previous literature [30]. The topmost valance band is stretching from -4.0 to 0 eV (Fermi level) and the conduction band is positioned at 3.19 eV above the Fermi level, suggesting that the estimated band gap has reproduced the experimental value of 3.19 [31] as depicted in Fig. 2a. Introducing Ti contents (0.125, 0.25, 0.500, 0.750 and 0.875) into the system would increase the intensity of states in the conduction and valence bands. However, the electronic band gap is reduced to 2.88, 2.67, 2.33, 2.28 and 2.19 eV at Ti loadings of 0.125, 0.25, 0.500, 0.750 and 0.875, respectively. This result indicates that Ti incorporation into ceria would induce an obvious band gap narrowing.

An investigation of Ti 3*d* orbital of each configuration was performed and the results are displayed in Fig. 3. The Ti 3*d* states in $Ce_{1-x}Ti_xO_2$ (x = 0.125, 0.250, 0.500, 0.750 and 0.875) systems are located at about similar energy range, suggesting that the Ti 3*d* states enhance gradually with increasing Ti concentrations. Moreover, the decrease in the band gap caused by the Ti incorporation is mainly due to increasing the Ti 3*d* states in the conduction band which is the core reason for enhancing the photocatalytic and optical activities of Ti-doped CeO_2.

For further underestanding the contribution of each of

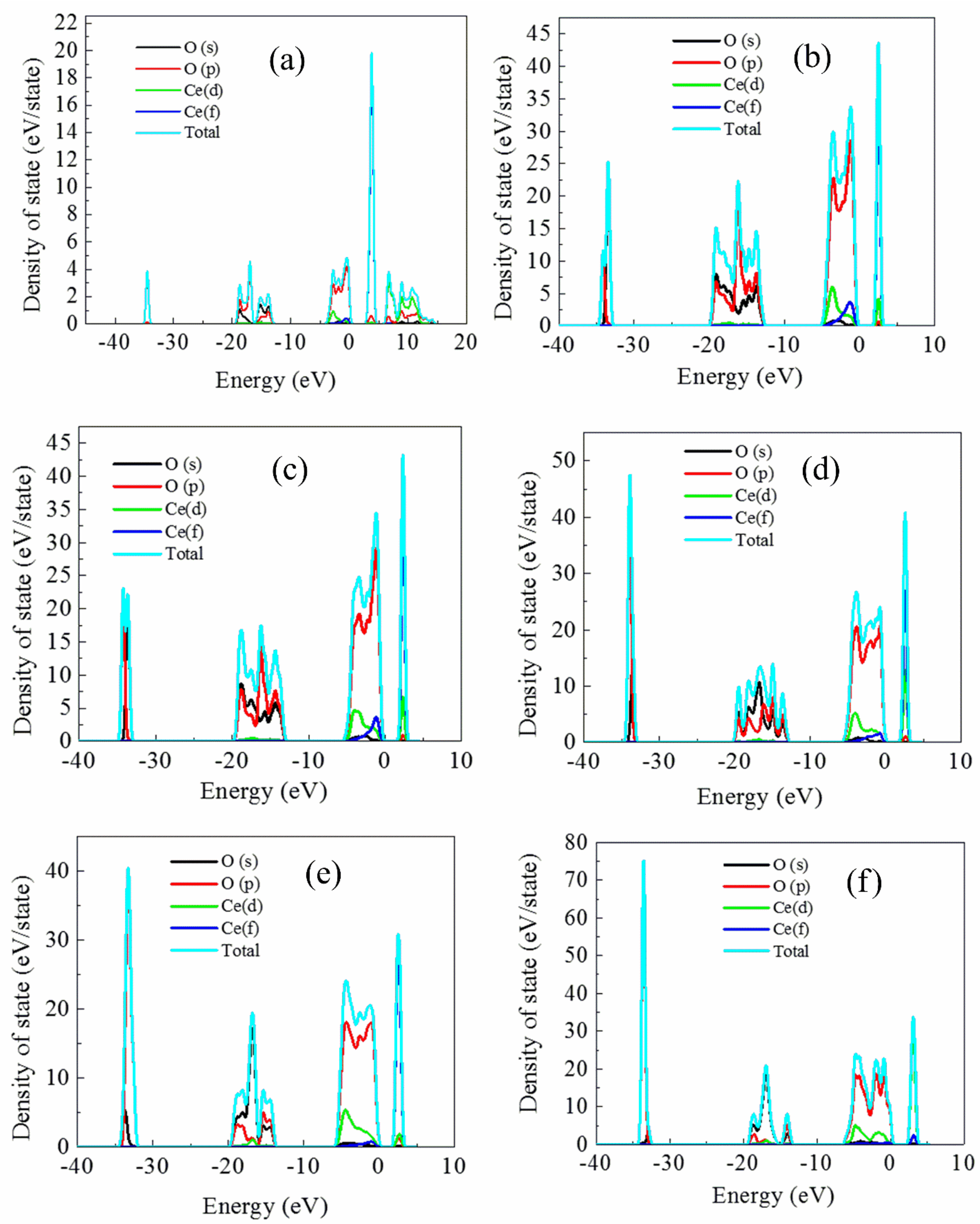

Fig. 2. The total and partial density of states (TPDOS) of $Ce_{1-x}Ti_xO_2$ system with (a) x = 0, (b) x = 0.125, (c) x = 0.250, (d) x = 0.500, (e) x = 0.750 and (f) x = 0.875.

the related orbitals to the partial density of states (PDOS), analysis of 5*d* and 4*f* orbitals of each configuration was performed and the results are dipicted in Fig. 4. At x = 0 (pure CeO_2), 4*f* orbitals of Ce atoms are predominant in the conduction band. However, the valence band is found to be mixed with both 4*f* and 5*d* orbitals.

Analysis of Optical Properties

It is well known that the strong light absorption is an indication of a high efficiency photocatalyst. The computed

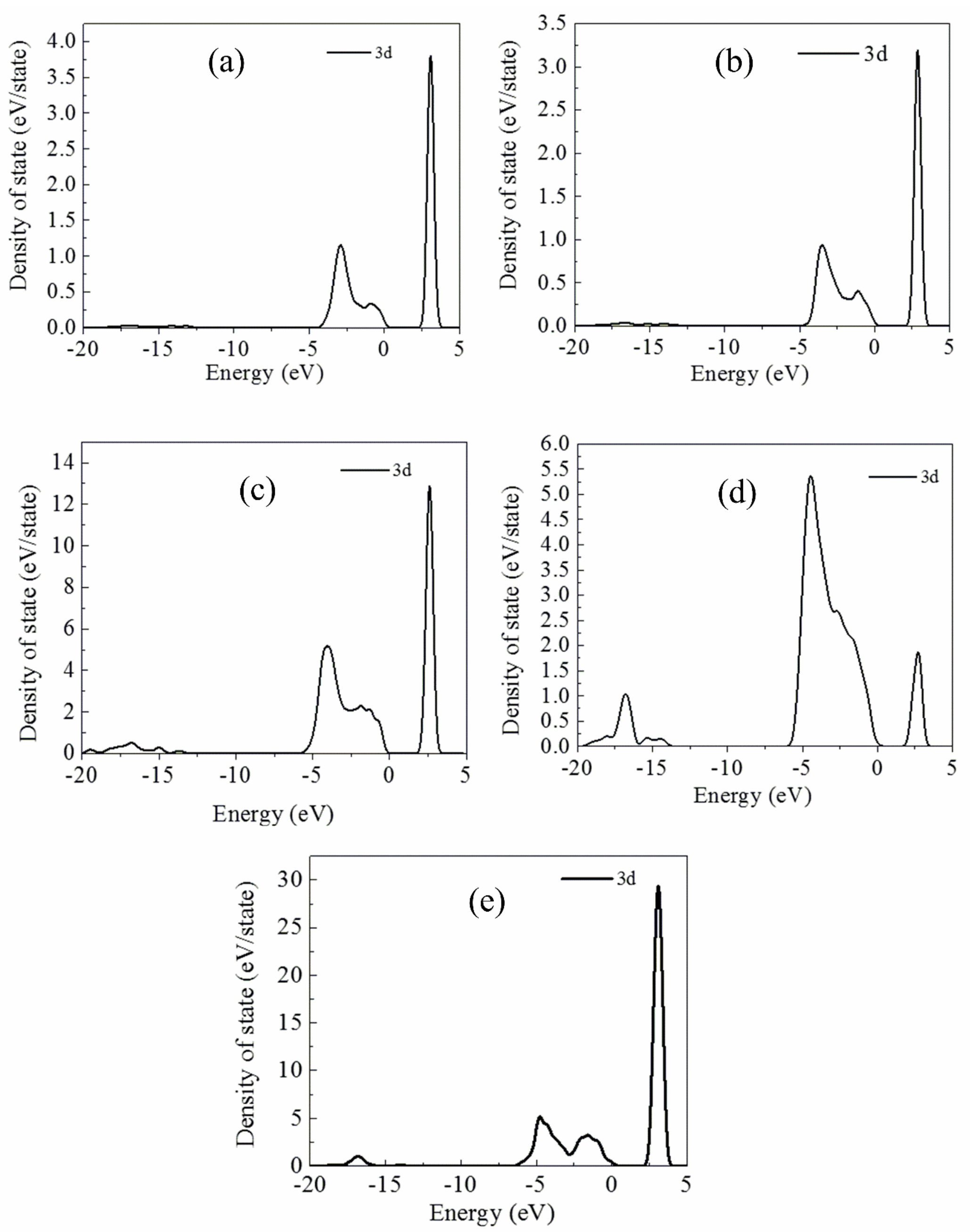

Fig. 3. 3*d* orbitals of Ti ion loadings at (a) x = 0.125, (b) x = 0.250, (c) x = 0.500, (d) x = 0.750 and (e) x = 0.875.

absorption coefficients of pure and Ti-modified CeO_2 configurations as a function of wavelength in the range of 200-1500 nm is depicted in Fig. 5. It is evident from the figure that pure CeO_2 spectrum shows a good absorption character for the incident photons in the ultra-violet part of the solar irradiation, whereas a slight component in the visible region is presented. However, the absorption edge shifted towards the visible light region when inserting Ti. This may be attributed to the incorporation of transition metals into the ceria lattice resulted in the formation of new

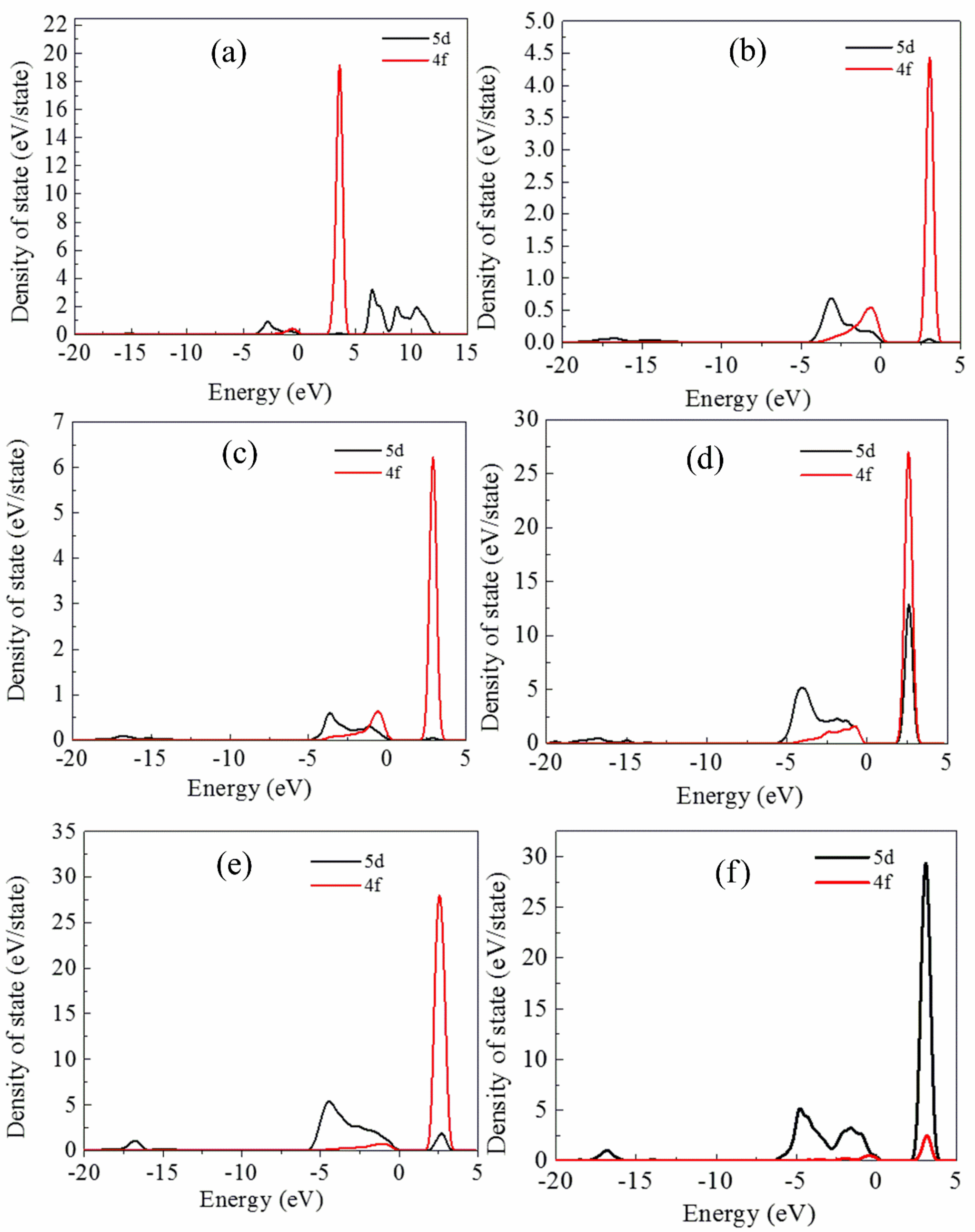

Fig. 4. 5*d* and 4*f* orbitals at Ti loadings of (a) x = 0, (b) x = 0.125, (c) x = 0.250, (d) x = 0.500, (e) x = 0.750, and (f) x = 0.875.

energy levels in the conduction band (Ti-3*d*) as demonstrated in Fig. 3. This in turn causes a red shift for the spectra, improving the photocatalytic performance of the studied systems. Furthermore, pure CeO_2 shows a good transparency in the visible range nominating this material for the optical applications. Furthermore, Ti-doped CeO_2 adsorption curves display relatively a comparable absorption values showing a good performance in the solar

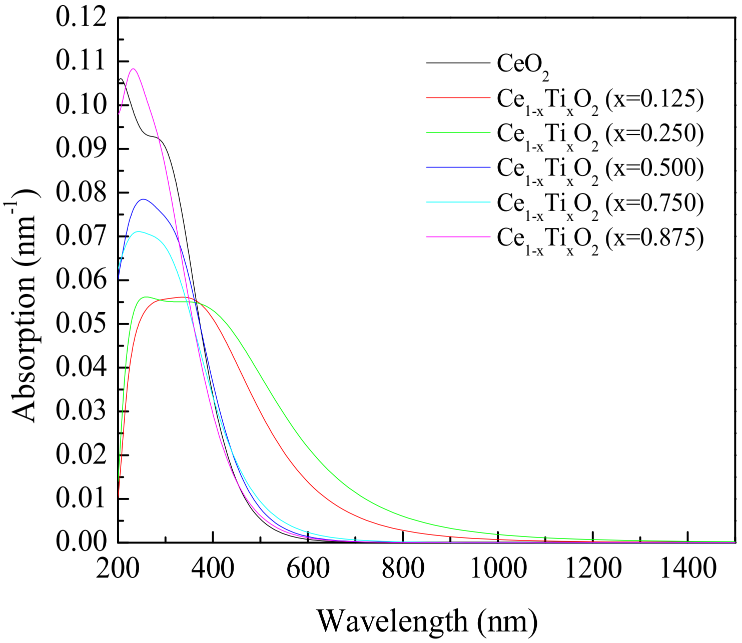

Fig. 5. The calculated optical absorption spectra of pure and Ti-doped CeO_2 configurations.

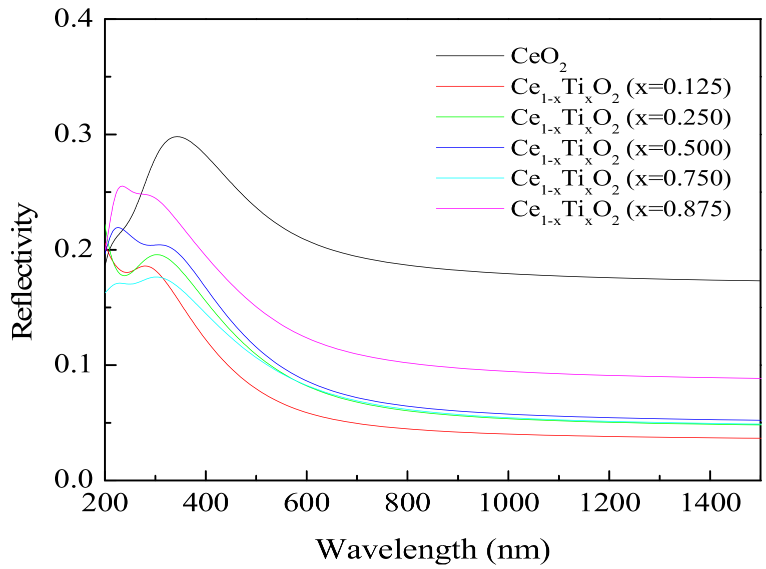

Fig. 6. Reflectivity spectra of pure CeO_2 and Ti-doped CeO_2 configurations.

cell applications [32].

It is well known that less reflectivity of a material exhibits high performance in solar cell applications. Reflectivity spectra for the considered systems are displayed in Fig. 6. The spectra demonstrate minimal values for the Ti-modified CeO_2 systems in the visible range of the

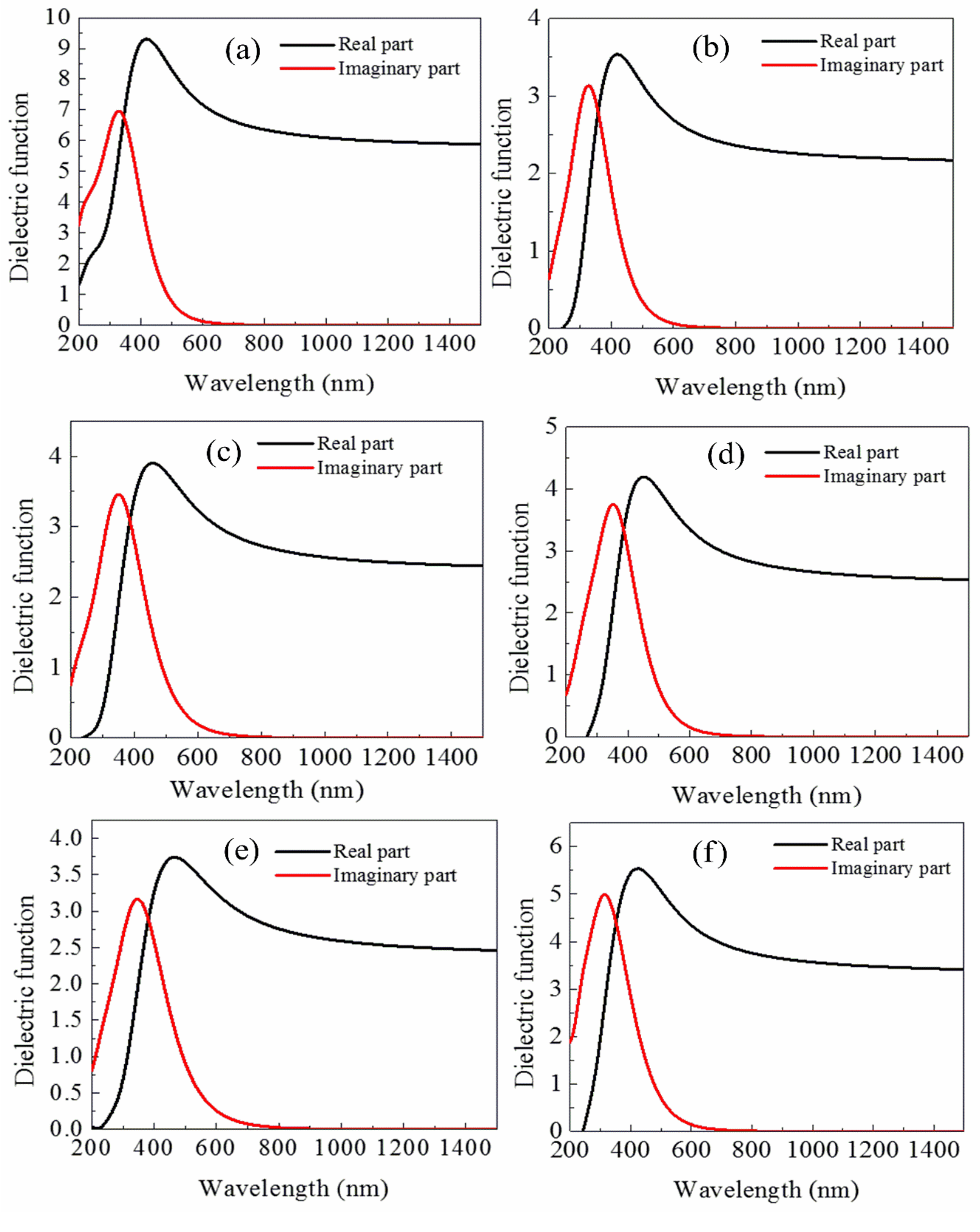

Fig. 7. The real and imaginary parts of dielectric function of $Ce_{1-x}Ti_xO_2$ at (a) x = 0, (b) x = 0.125, (c) x = 0.25, (d) x = 0.500, (e) x = 0.750, and (f) x = 0.875.

electromagnetic waves (EM). This reduction in reflectivity is extended to some UV reign, reflecting good characters for such materials. The DFT computed absorption and reflectivity spectra of pure CeO_2 exhibit a similar trend with our previous experimental work [32] in the wavelength range between 200 and 1500 nm. Both theoretical and measured results have peaks in shorter wavelengths.

The dielectric function corresponds to the interaction between the incident photons and electrons in a material. Optical transitions between occupied and unoccupied states are caused by the electric field of the photon. The spectra from the excited states can be identified as a joint density of states between the valence and conduction bands [26]. The dielectric functions involve two effects which are intraband effects from the contribution of free electrons and interband effects from the contribution of valance electrons [33]. The imaginary part of the dielectric function $\varepsilon_2(\omega)$ can be computed from the momentum matrix elements between the occupied and unoccupied wave functions [27]. The real part $\varepsilon_1(\omega)$ of the dielectric function can be assessed from the imaginary part $\varepsilon_2(\omega)$ by Kramer-Kronig transformation [34]. The wavelength dependent spectra of the real and imaginary parts of the complex dielectric function of pure and doped CeO_2 are depicted in Fig. 7. The obvious zero values of $\varepsilon_2(\omega)$ at wavelengths longer than 650 nm demonstrate a high-quality transparent material for optical applications [32].

CONCLUSIONS

This is a report of a first-principle study to evaluate the effect of Ti-insertion on the electronic and optical properties of CeO_2. The obtained results suggested that the Ti incorporation into ceria could evidently induce band gap narrowing to 2.88, 2.67, 2.33, 2.28 and 2.19 eV at Ti contents of 0.125, 0.25, 0.500, 0.750 and 0.875 correspondingly. Furthermore, Ti-doping introduces 3*d* states in the conduction band of CeO_2. The 3*d* states play an important role on reducing the band gap. Moreover, the optical absorption shifts to a longer wavelength range indicating the possible applications as a photocatalytic material. Analysis of Mulliken charges suggests an ionic character for Ce-O and Ti-O bonds, while a covalent character was found for the Ce-Ti bond.

REFERENCES

[1] Sato, S.; Takahashi, R.; Kobune, M.; Gotoh, H., Basic properties of rare earth oxides. *Appl. Catal. A: Gen.* **2009**, *356*, 57-63. DOI: 10.1016/j.apcata.2008.12.019.

[2] Azimi, G.; Dhiman, R.; Kwon, H. -M.; Paxson, A. T.; Varanasi, K. K., Hydrophobicity of rare-earth oxide ceramics, *Nat. Mater.* **2013**, *12*, 315-320. DOI: 10.1038/nmat3545.

[3] Suzuki, C.; Kawai, J.; Takahashi, M.; Vlaicu, A. -M.; Adachi, H.; Mukoyama, T., The electronic structure of rare-earth oxides in the creation of the core hole. *Chem. Phys.* **2000**, *253*, 27-40. DOI: 10.1016/S0301-0104(99)00380-8.

[4] Casadei, M.; Ren, P.; Rinke, Rubio, A.; Scheffler, M., Density-functional theory for f-electron systems: The α-γ phase transition in cerium. *Phys. Rev. Lett.* **2012**, *109*, 146402. DOI: 10.1103/PhysRevLett.109.146402.

[5] Wu, X. D.; Dye, R. C.; Muenchausen, R. E.; Foltyn, S. R.; Maley, M.; Rollett, A. D.; Garcia, A. R.; Nogar, N. S., Epitaxial CeO_2 films as buffer layers for high-temperature superconducting thin films. *Appl. Phys. Lett.* **1991**, *58*, 2165-2167. DOI: 10.1063/ 1.104994.

[6] Kharton, V. V.; Figueiredo, F. M.; Navarro, L.; Naumovich, E. N.; Kovalevsky, A. V.; Yaremchenko, A. A.; Viskup, A. P.; Carneiro, A.; Marques, F. M. B.; Frade, J. R., Ceria-based materials for solid oxide fuel cells. *J. Mater. Sci.* **2001**, *36*, 1105-1117. DOI: 10.1023/A:1004817506146.

[7] Ibrahim, M. I.; Safi, A. A., The effect of rear earth doping CdS nanostructure on structural, optical and photoconductivity properties. *IJP*. **2019**, *17*, 108-118. DOI: 10.20723/ijp.17.40.108-118.

[8] Al-Mashhadani, A. H.; Yas, R. M.,Study of *in vitro* and *in vivo* free radical scavenging activity for radioprotection of cerium oxide nanoparticles, *IJP*. **2017**, *15*, 40-47. DOI: 10.30723/ijp.v15i35.52.

[9] Thammachart, M.; Meeyoo, V.; Risksomboon, T.; Osuwan, S., Catalytic activity of CeO_2-ZrO-mixed oxide catalysts prepared *via* sol-gel technique: CO oxidation, *Catal.* **2001**, *68*, 53-61. DOI: 10.1016/ S0920-5861(01)00322-4.

[10] Miran, H. A.; Altarawneh, M.; Jiang, Z. -T.; Oskierski, H.; Almatarneh, M.; Dlugogorski, B. Z., Decomposition of selected chlorinated volatile organic compounds by ceria (CeO_2). *Catal. Sci. Technol.* **2017**, *7,* 3902-3919. DOI: 10.1039/ c7cy01096f.

[11] Orel, Z. C.; Orel, B., Optical properties of pure CeO_2 and mixed CeO_2/SnO_2 thin film coatings, *Phys. Status Solidi (b)*, **1994**, *186*, K33-K36. DOI: 10.1002/ pssb.2221860135.

[12] Dao, N. N.; Luu, M.; Dai, Nguyen, Q. K.; Kim, B. S.,

UV absorption by cerium oxide nanoparticles/epoxy composite thin films. *Adv. Nat. Sci: Nanosci. Nanotechnol.* **2011**, 2, 045013. DOI: 10.1088/2043-6262/2/4/045013.

[13] Yue, L.; Zhang, X. -M., Structural characterization and photocatalytic behaviors of doped CeO_2 nanoparticles. *J. Alloys Compd.* **2009**, *475*, 702-705. DOI: 10.1016/j.jallcom.2008.07.096.

[14] Truffault, L.; Ta, M. T.; Devers, T.; Konstantinov, K.; Harel, V.; Simmonard, C.; Andreazz, C.; Nevirkovetsb, I. P.; Pineau, A.; Veron, O.; Blondeau, J. -P., Application of nanostructured Ca doped CeO_2 for ultraviolet filtration. *Mater. Res. Bull.* **2010**, *45*, 527-535. DOI: 10.1016/j.materresbull.2010.02.008.

[15] Channei, D.; Inceesungvorn, B.; Wetchakun, N.; Ukritnukun, S.; Nattestad, N.; Chen, J.; Phanichphant, S., Photocatalytic degradation of methyl orange by CeO_2 and Fe-doped CeO_2 films under visible light irradiation. *Sci. Rep.,* **2014**, *4*, 5757. DOI: 10.1038/srep05757.

[16] Liyanage, A. D.; Perera, S. D.; Tan, K.; Chabal, Y.; Balkus Jr, K. J., Synthesis, characterization, and photocatalytic activity of Y-doped CeO_2 nanorods. *ACS Catal.* **2014**, *4*, 577-584. DOI: 10.1021/cs400889y.

[17] Soni, S.; Kumar, S.; Dalela, B.; Kumar, S.; Alvi, P.; Dalela, S., Defects and oxygen vacancies tailored structural and optical properties in CeO_2 nanoparticles doped with Sm^{3+} cation. *J. Alloys Compd.* **2018**, *752*, 520-531. DOI: 10.1016/j.jallcom.2018.04.157.

[18] Zhao, S.; Kang, D.; Liu, Y.; Wen, Y.; Xie, X.; Yi, H.; Tang, X., Spontaneous formation of asymmetric oxygen vacancies in transition-metal-doped CeO_2 nanorods with improved activity for carbonyl sulfide hydrolysis. *ACS Catal.* **2020**, *10*, 11739-11750. DOI: 10.1021/acscatal.0c02832.

[19] Ranjith, K. S.; Dong, C. -L.; Lu, Y. R.; Huang, Y. -C.; Chen, C. -L., Saravanan, P.; Asokan, K.; Rajendra Kumar, R. T., Evolution of visible photocatalytic properties of Cu-doped CeO_2 nanoparticles: Role of Cu^{2+}-mediated oxygen vacancies and the mixed-valence states of Ce ions, ACS Sustain. *Chem. Eng.* **2018**, *6*, 8536-8546. DOI: 10.1021/acssuschemeng.8b00848.

[20] Yang, K.; Li, D. -F.; Huang, W. -Q.; Xu, L.; Huang, G. -F.; Wen, S., Origin of enhanced visible-light photocatalytic activity of transition-metal (Fe, Cr and Co)-doped CeO_2: Effect of 3d orbital splitting. *Appl. Phys. A*, **2017**, *123*, 96. DOI: 10.1007/s00339-016-0700-9.

[21] Basharnavaz, H.; Habibi-Yangjeh, A.; Kamali, S. H., Adsorption performance of SO_2 gases over the transition metal/P-codoped graphitic carbon nitride: a DFT investigation. *Mater. Chem. Phys.* **2020**, *243*, 122602. DOI: 10.1016/j.matchemphys.2019.122602.

[22] Basharnavaz, H.; Habibi-Yangjeh, A.; Mousavi, M., Ni, Pd, and Pt-embedded graphitic carbon nitrides as excellent adsorbents for HCN removal: a DFT study, *Appl. Surf. Sci.* **2018**, *456*, 882-889. DOI: 10.1016/j.apsusc.2018.06.159.

[23] Miran, H. A.; Altarawneh, M.; Widjajaa, H.; Jaf, Z. N.; Rahman, M. M.; Vedere, J. -P.; Dlugogorskic, B. Z.; Jiang, Z. T., Thermo-mechanical properties of cubic lanthanide oxides. *Thin Solid Films.* **2018**, *653*, 37-48. DOI: 10.1016/j.tsf.2018.01.063.

[24] Segall, M. D.; Philip, J. D.; Lindan; M. J.; Probert; C. J.; Pickard, P. J.; Hasnip, S. J.; Clark, Payne, M. C., First-principles simulation: ideas, illustrations and the CASTEP code. *J. Phys. Condens. Matter*. **2002**, *14*, 2717. DOI: 10.1088/0953-8984/14/11/301.

[25] Cohen, A. J.; Mori-Sánchez, P.; Yang, W., Insights into current limitations of density functional theory. *Science*, **2008**, *321*, 792-794. DOI: 10.1126/science.1158722.

[26] Zhang, X. D.; Guo, M. L.; Liu, C. L.; Zhang, L. A.; Zhang, W. Y.; Ding, Y. Q.; Wu, Q.; Feng, X., First-principles investigation of electronic and optical properties in wurtzite Zn1-xMg xO, *Eur. Phys. J. B*, **2008**, *62*, 417-421. DOI: 10.1140/epjb/e2008-00186-9.

[27] Fu, C.; Li, T.; Qi, J.; Pan, J.; Chen, S.; Cheng, C., Theoretical study on the electronic and optical properties of Ce^{3+}-doped TiO_2 photocatalysts. *Chem. Phys. Lett.* **2010**,*494*, 117-122, DOI: 10.1016/j.cplett.2010.05.085.

[28] Xue, Y.; Tian, Y.; Zhang, D.; Zeng, C.; Fu, Y.; Li, K.; Wang, H.; Tian, Y., The mechanism of photocatalyst and the effects of co-doping CeO_2 on

refractive index and reflectivity from DFT calculation. *Comput. Mater. Sci.* **2019**, *158*, 197-208. DOI: 10.1016/j.commatsci.2018.11.003.

[29] Lawler, R.; Cho, J.; Ham, H. C.; Ju, H.; Lee, W. S.; Kim, J. Y.; Choi, J. ll.; Jang, S. S., CeO_2 (111) Surface with oxygen vacancy for radical scavenging: a density functional theory approach. *J. Phys. Chem. C,* **2020**, *124*, 20950-20959. DOI: 10.1021/acs.jpcc.0c05717.

[30] Loschen, C.; Carrasco, J.; Neyman, K. M.; Illas, F., First-principles LDA + U and GGA + U study of cerium oxides: Dependence on the effective U parameter. *Phys. Rev. B,* **2007**, *75*, 035115. DOI: 10.1103/PhysRevB.75.035115.

[31] Skorodumova, N.; Ahuja, R.; Simak, S.; Abrikosov, I.; Johansson, B.; Lundqvist, B., Electronic, bonding, and optical properties of CeO_2 and Ce_2O_3 from first principles. *Phys. Rev. B,* **2001**, *64*, 115108. DOI: 10.1103/PhysRevB.64.115108.

[32] Miran, H. A.; Jiang, Z. -T.;Altarawneh, M.; Veder, J. P.; Zhou, Z. -F.; Rahman, M. M.; Jaf, Z. N.; Dlugogorski, B. Z., Influence of DC magnetron sputtering reaction gas on structural and optical characteristics of Ce-oxide thin films. *Ceram. Int.* **2018**, *44*, 16450-16458. DOI: 10.1016/j.ceramint.2018.06.059.

[33] Jaf, Z. N.; Jiang, Z. -T.; Miran, H. A.; Altarawneh, M., Thermo-elastic and optical properties of molybdenum nitride. *Can. J. Phys.* **2016**, *94*, 902-912, DOI: 10.1139/cjp-2016-0125.

[34] Dressel, M.; Gompf, B.; Faltermeier, D.; Tripathi, A.; Pflaum, J.; Schubert, M., Kramers-Kronig-consistent optical functions of anisotropic crystals: generalized spectroscopic ellipsometry on pentacene. *Opt. Express* **2008**, *16*, 19770-19778. DOI: 10.1364/OE.16.019770.